Environmental Research 197 (2021) 111107

Contents lists available at ScienceDirect

Environmental Research

journal homepage: www.elsevier.com/locate/envres

Prediction of batch sorption of barium and strontium from saline water

B.S. Reddy [a,1], A.K. Maurya [b,1], Sathishkumar V E [c], P.L. Narayana [b], M.H. Reddy [d], Alaa Baazeem [e], Kwon-Koo Cho [a,*], N.S. Reddy [b,**]

[a] Department of Materials Engineering and Convergence Technology & RIGET, Gyeongsang National University, Jinju, 52828, South Korea
[b] School of Materials Science and Engineering, Engineering Research Institute, Gyeongsang National University, Jinju, 52828, South Korea
[c] Department of Computer Science and Engineering, Kongu Engineering College, Perundurai, Erode, 638101, Tamilnadu, India
[d] Department of Mechanical Engineering, St. Peter's Engineering College, Hyderabad, India
[e] Department of Biology, College of Science, Taif University, P.O. Box 11099, Taif, 21944, Saudi Arabia

ARTICLE INFO

Keywords:
Artificial neural networks
Prediction
Sorption
Sensitivity analysis
Saline water
Petroleum industries

ABSTRACT

Celestite and barite formation results in contamination of barium and strontium ions hinder oilfield water purification. Conversion of bio-waste sorbent products deals with a viable, sustainable and clean remediation approach for removing contaminants. Biochar sorbent produced from rice straw was used to remove barium and strontium ions of saline water from petroleum industries. The removal efficiency depends on biochar amount, pH, contact time, temperature, and Ba/Sr concentration ratio. The interactions and effects of these parameters with removal efficiency are multifaceted and nonlinear. We used an artificial neural network (ANN) model to explore the correlation between process variables and sorption responses. The ANN model is more accurate than that of existing kinetic and isotherm equations in assessing barium and strontium removal with adj. R^2 values of 0.994 and 0.991, respectively. We developed a standalone user interface to estimate the barium and strontium removal as a function of sorption process parameters. Sensitivity analysis and quantitative estimation were carried out to study individual process variables' impact on removal efficiency.

1. Introduction

The water produced from oil and gas reservoirs comprises organic chemicals, mineral ions (Na^+, Ca^{2+}, Mg^{2+}, CO_3^{2-}, and SO_4^{2-}), dissolved salts (NaCl), heavy metals, and other radioactive metallic ions such as barium and strontium (Ba(II), and (Sr(II)) than the maximum contaminant levels for drinking water (Yost et al., 2016; Zhai et al., 2021). Among all those elements, the radioactive Ba(II) and Sr(II) toxic ions come from nuclear weapon testing, power plant, research facilities, and mines (Prelot et al., 2018). The continuous discharge of fluid waste will spread into the environment and harms the natural water bodies, wildlife, agriculture, and human health (Al-Ghouti et al., 2019; Kaveeshwar et al., 2018; Reddy et al., 2021b). Moreover, the Ba(II)/Sr(II) ions will harm the desalination system (damages in reverse osmosis membranes) due to the interactions of the CO_3^{2-}, and SO_4^{2-} anions in underground/seawater to form mineral scale fouling (Zhang et al., 2019). In the petroleum industry, the re-injection of oilfield-produced water is limited due to mineral scale formation (Ayirala et al., 2018; Katende and Sagala, 2019; Sivalingam et al., 2019). The strontium and barium sulfate are some of the most dominant mineral scale deposits in oilfield water due to low solubility, high hardness, high resistance to chemical treatments (Kamal et al., 2018). It is essential to remove Ba(II)/Sr(II) ions before discharging them into the environment and water. These scales are formed by the injection of low-quality water comprising high absorptions of Sr(II)/Ba(II) cations with the downstream formation of water containing sulfate ions (Bukuaghangin et al., 2016). Therefore, it is essential to control the generation of sulfate scales for improving the production of clean water.

There are several techniques used to reduce the formation of sulfate scale, for instance, the flow filtration process (like membrane separations, adsorption columns, and sand filters), chemical scale inhibitors, sorption, and batch separation (skimmers, chemical precipitation tanks, and API separators) (Fakhru'l-Razi et al., 2009; Fard et al., 2017; Kamal et al., 2018; Nishiyama et al., 2016). Among all, the sorption technique

* Corresponding author.
** Corresponding author.
E-mail addresses: kkcho66@gnu.ac.kr (K.-K. Cho), nsreddy@gnu.ac.kr (N.S. Reddy).
[1] Equally contributed.

https://doi.org/10.1016/j.envres.2021.111107
Received 3 March 2021; Received in revised form 24 March 2021; Accepted 25 March 2021
Available online 1 April 2021

Table 1
Statistics of the input and output variables used in the current study.

Variables	Minimum	Mean	Maximum	Std. Dev
Biochar (g/L)	1	3	5	1.6
pH	3	6	9	2.5
Temperature (°C)	20	35	50	12.4
Time (h)	1	12.5	24	9.5
Ba/Sr ratio	0.1	50	100	41.2
Sorption of Ba(II) (μmol/g)	1.4	118.3	871	203.4
Sorption of Sr(II) (μmol/g)	2.3	189.55	1157.8	270.8

is widely used to remove the Ba(II) and Sr(II) ions from the oilfield-produced water (Younis et al., 2017). However, the sorption technique is expensive, and researchers focused on preparing cheap biochar as carbon-based sorbents made from agricultural wastes (Li et al., 2019; Younis and Moustafa, 2017). Biochar sorbents successfully played a crucial role in removing organic pollutants and heavy metals from the wastewater (El-Salamony et al., 2017; Mohubedu et al., 2019; Zhou et al., 2019). Biochar produced from rice straw was used for the removal of Ba(II)/Sr(II) ions from oilfield effluent water treatment (Rashidi and Yusup, 2017). The sorption efficiency of the Ba(II)/Sr(II) depends on the biochar (g/L), pH, temperature (°C), time (h), and Ba/Sr ratios. It is crucial to know the influence of the sorption conditions to achieve high ion removal efficiency. However, it is challenging to optimize sorption conditions for higher efficiency due to nonlinear and complex relations among the process parameters. Developing mathematical equations based on adsorption kinetics and isotherm equations is laborious and time-consuming. Therefore, there is a need for a computational study to understand the complex and nonlinear relationships among the process parameters and removal efficiency. Data based artificial neural network (ANN) method is an appropriate tool to analyze the sorption relationship. ANN has been successfully used for predicting the Zn(II) ion removal (Hoseinian et al., 2020), heavy metals (Nieva et al., 2020), and the Cr(VI) removal (Nag et al., 2020) from wastewater and achieved good accuracy.

In this work, we present an ANN approach to the sorption process for Ba(II)/Sr(II) ions removal from saline water by using rice straw-based biochar. We developed a systematic ANN framework to determine the relationship among batch adsorption input variables on the removal of Ba(II)/Sr(II). The considered process variables are biochar amount, pH, contact time, temperature, and Ba/Sr concentration ratio. The specific objectives of the present work are:

(1) To compare the ANN predicted results with experimental observations, predictions from RSM, kinetic and isotherm equations.
(2) To develop user-friendly ANN software for Ba(II)/Sr(II) removal efficiency for easy use based on the best architecture weights.
(3) Sensitivity analysis and virtual experimentation method used to study the impact of process variables on removal efficiency.

2. Materials and methods

2.1. Experimental data

The biochar sorbent was prepared by using rice straw. (Younis et al., 2020). Total 30,000 mg/L (pH = 6) total dissolved solids (TDS) saline water solution simulates the oilfield wastewater real composition. The composition of TDS in this saline solution was made to contain 50% anionic (45% Cl^- and 5% (HCO^{3-} and SO^{2-}_4) and 50% cationic constituents (40% (Na^++K^+), 9.5% (Ca^{2+}+Mg^{2+}), and 0.5% (Ba^{2+}+S^{2+})) based on molecular weight. The input variables are biochar (1–5 g/L), pH (3–9), temperature (20–50 °C), time (1–24 h), and Ba/Sr ratio (0.1–100%), and the output variables are Ba(II) and Sr(II), respectively. The experimental data of the TDS saline water contains biochar (g/L), pH, temperature (°C), time (h), and Ba/Sr ratios (%) and respective % removal of barium (Ba(II)) and strontium (Sr(II)). The data consists of 50 experimental conditions; from the complete database, we divided 80% (40 datasets) to develop the ANN model and 20% (10 datasets) to validate the model performance. The statistics and the total datasets were presented in Table 1&2.

2.2. Artificial neural network (ANN) model development

An ANN, inspired by the human brain, is a dominant modeling technique for linear or nonlinear relationships, capturing and representing complex input/output associations (Hasson et al., 2020). The unique features of ANN like parallelism, consistency, training, learning, and generalization made it an appropriate tool for a wide range of

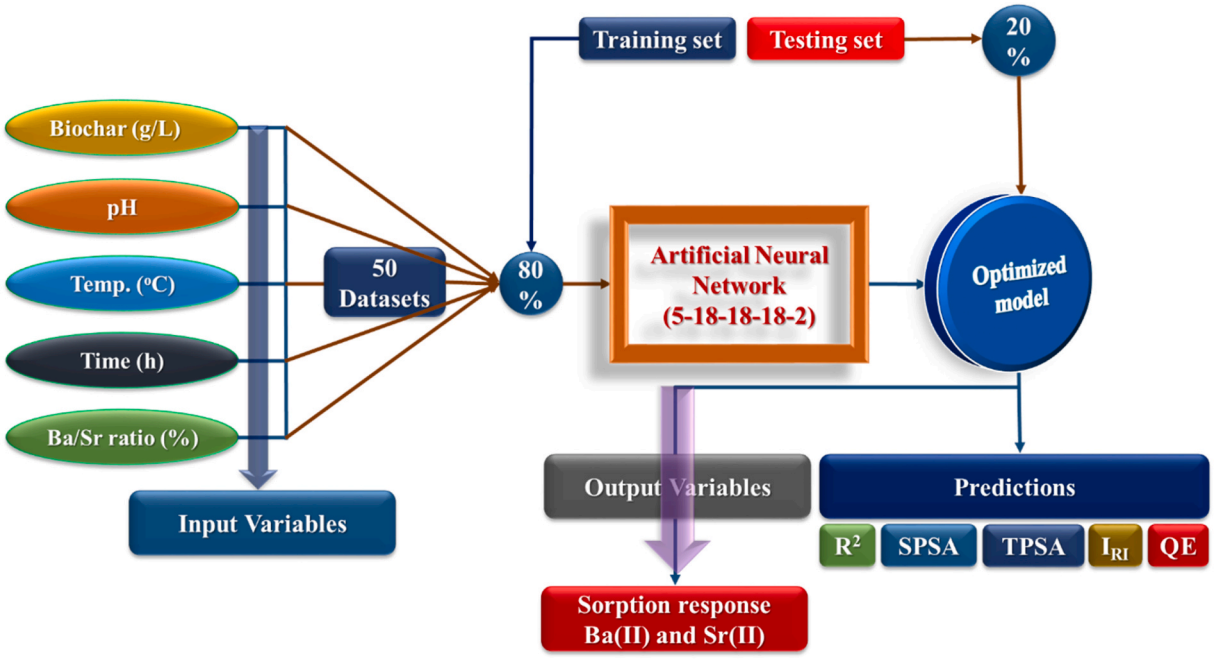

Fig. 1. Schematic representation of the proposed ANN model.

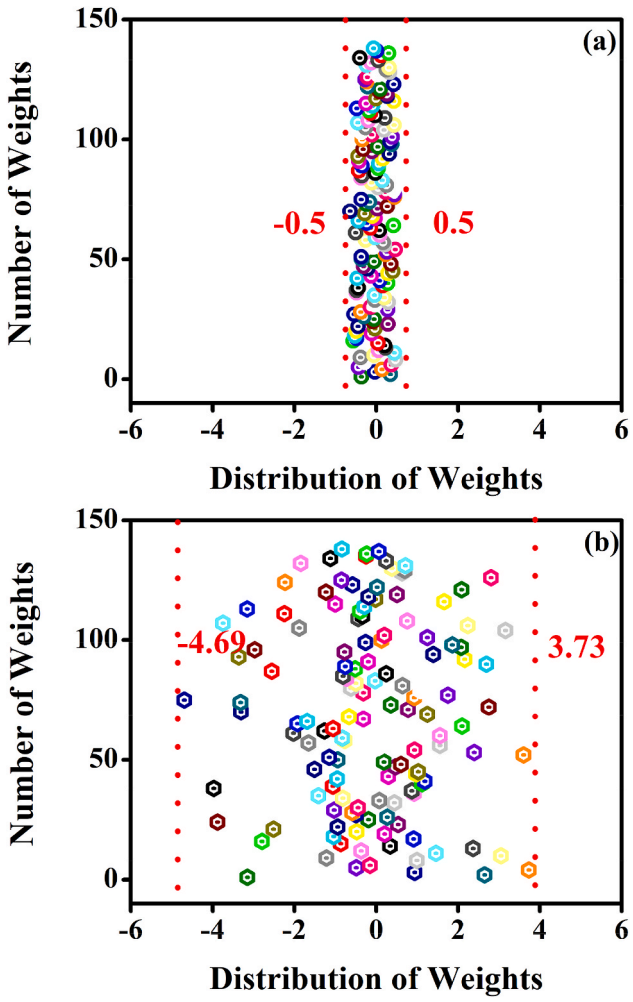

Fig. 2. Distribution of weights (a) initial and (b) best model weights (5-8-8-2) of the removal of Ba(II)/Sr(II).

problems such as classification, prediction, filtering, function approximation, and recognition. There are many ANN techniques; in the present work, we used Feed Forward Neural Network with backpropagation algorithm.

Fig. 1 shows the illustration of the current study's detailed ANN procedure. The process parameters (inputs) and Ba(II) and Sr(II) (outputs) data were normalized between 0.1 and 0.9 by using a normalizing equation before using in the network (Reddy et al., 2020; Sadan et al., 2016). The ANN program was written in C language, and the corresponding graphical user interface (GUI) was designed in the JAVA program (Reddy et al., 2015, 2021a). The ANN model was trained with the backpropagation algorithm with a sigmoid activation function (Lippmann, 1987). To obtain the model's best architecture, we varied hidden layers, neurons in the hidden layer, and the hyperparameters (learning rate, momentum term, and iterations) and evaluated the root mean square error (RMSE), adj. R^2 and Pearson's r along with the average error in output predictions (MAE).

To obtain the best architecture, first, the model was tested with different hidden layers (one, two, and three) consists of 2–20 hidden neurons at a constant momentum term (0.3), learning rate (0.5), and iterations (5000). The two hidden layers with eight hidden neurons achieved absolute minimum error, as shown in Fig. S1 (see in supplementary file). The 5-8-8-2 architecture was trained with varying momentum term and learning rate (0.1–0.9). We found the absolute minimum error with the momentum of 0.8 and learning rate of 0.5, as shown in Fig. S2 & S3. Finally, we changed the iterations from 0 to 8000; at 6000 iterations, we achieved the minimum RMSE and average error shown in Fig. S4. We concluded that the best model has a 5-8-8-2 architecture with a momentum term of 0.7 and a learning rate of 0.7 at 6000 iterations.

2.3. Transformation of network weights

The ANN model communicates the input and output data by transforming coefficients and holds the evidence about the association between process variables and Ba(II) and Sr(II) removal. Each neuron is associated with a different transformation of weights, which designates the asset between the process variables and output variables. Fig. 2 (a&b) shows the initial and final change of coefficients after 6000

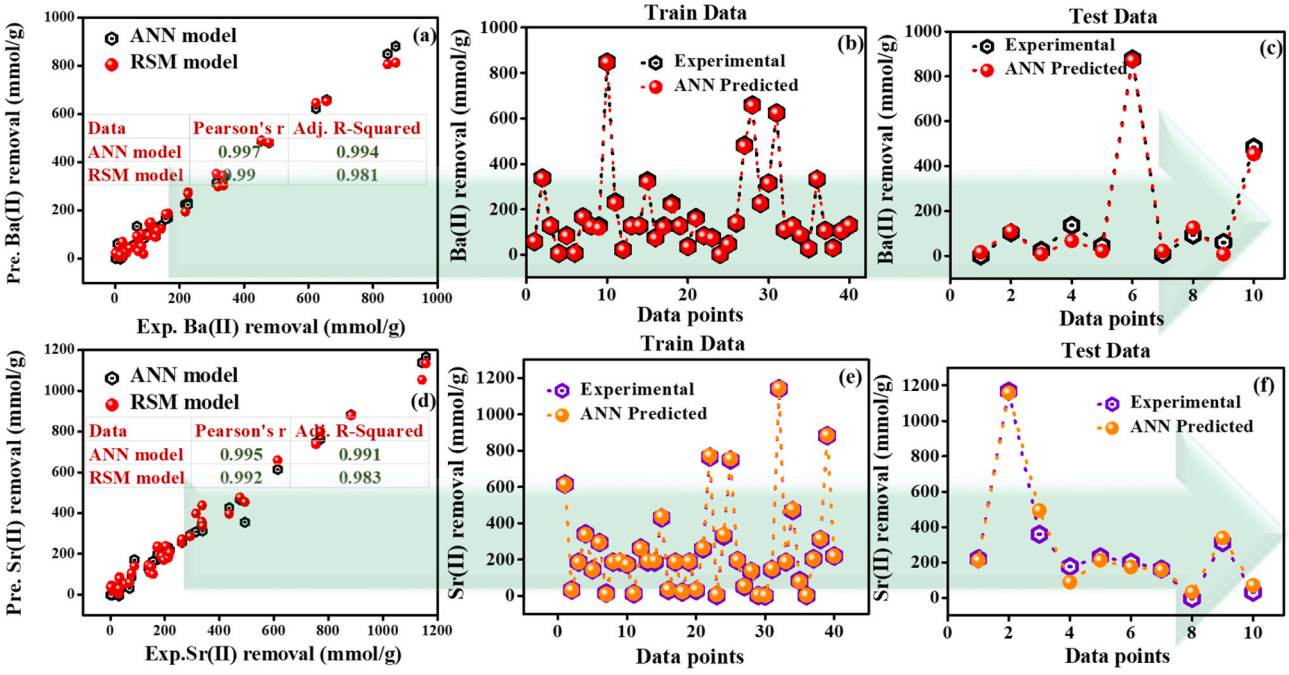

Fig. 3. Comparison between the experimental removal of Ba(II) and Sr(II) with the ANN model and published the RSM model.

Table 2
The experimental conditions and respective observation comparisons with the existing RSM model (Younis et al., 2020) and ANN model. **Bold (41–50)** datasets are considered as test datasets.

S.No	Biochar (g/L)	pH	Temp. (oC)	Time (h)	Ba/Sr ratio (%)	Ba(II) removal			Sr(II) removal		
						Exp.	*RSM*	*ANN*	*Exp.*	*RSM*	*ANN*
1.	1	9	20	1	0.1	58.9	50.9	58.093	614.1	658.3	614.75
2.	3	6	35	12.5	100	336.6	303.6	338.274	31.1	4.2	32.631
3.	3	6	35	12.5	50	127.4	120	127.502	185.2	188.9	186.027
4.	5	9	50	24	0.1	5.7	29.9	7.118	337.1	437.3	341.149
5.	5	6	35	12.5	50	82	52.3	85.606	143.6	109.9	144.48
6.	3	6	35	12.5	50	127.7	120	125.8	189.2	188.9	187.2
7.	5	9	50	1	0.1	7.3	8.8	7.522	293.3	286.3	293.64
8.	5	3	50	24	100	164.5	187.6	167.094	9.5	16.7	15.454
9.	3	6	35	12.5	50	125.8	120	127.502	187.2	188.9	186.027
10.	3	6	35	12.5	50	116	120	127.502	194.9	188.9	186.027
11.	1	9	50	24	100	846	806.1	848.226	173	230.4	173.503
12.	1	3	50	1	0.1	88.3	19.6	85.483	476.7	478	469.899
13.	5	9	20	24	100	226.3	276.3	232.263	14	37.7	11.407
14.	5	3	20	24	0.1	21	8.5	23.337	262	257.2	263.041
15.	3	6	35	12.5	50	125.6	120	127.502	192.7	188.9	186.027
16.	3	6	35	12.5	50	128.1	120	127.502	193.6	188.9	186.027
17.	1	6	35	12.5	50	319.1	299.1	325.932	436.8	396.5	429.45
18.	3	6	35	1	50	27.9	54.5	27.185	78.4	105.6	84.491
19.	5	3	20	1	100	71.8	31.6	75.845	34.6	86.9	29.647
20.	3	6	35	12.5	50	120.6	120	127.502	188.3	188.9	186.027
21.	5	3	20	24	100	218.2	194.7	225.039	23.2	24.1	20.896
22.	3	6	35	12.5	50	127.8	120	127.502	189.9	188.9	186.027
23.	5	3	50	1	100	34.8	24.5	37.169	34.6	79.4	29.123
24.	1	3	50	1	100	334.1	345.7	332.312	3.3	44	1.465
25.	3	6	35	24	50	157.5	185.5	164.165	263.3	272.1	257.877
26.	1	3	20	24	0.1	82.1	103.5	84.52	771.3	798.9	764.612
27.	5	9	50	1	100	73	83.8	75.826	7.3	−22.5	1.553
28.	5	9	20	24	0.1	1.4	22.8	2.514	336.4	357.6	328.637
29.	1	9	50	1	0.1	45.3	43.9	46.726	755	737.9	747.714
30.	3	9	35	12.5	50	105.7	146.4	107.919	203.6	238.4	204.115
31.	3	6	20	12.5	50	142.2	123.5	139.672	196.8	170.8	193.761
32.	1	9	50	1	100	477.9	482.9	482.128	54.8	53.6	49.806
33.	1	3	20	24	100	655.9	653.6	659.449	139.2	145.3	134.24
34.	5	9	50	24	100	226	269.2	225.977	5.2	45.2	1.082
35.	1	3	20	1	100	314.4	352.7	315.813	2.3	36.5	−0.981
36.	1	3	20	1	0.1	29	26.7	31.197	314.3	398.4	310.028
37.	5	9	20	1	0.1	16.1	15.8	−0.1	210.8	206.7	220.414
38.	1	9	50	24	0.1	110	143	103.357	1157.8	1133.5	1167.44
39.	3	6	35	12.5	0.1	7.7	−9.0	24.284	493.3	454.5	359.196
40.	3	3	35	12.5	50	66.8	93.5	136.081	88.3	139.3	175.547
41.	**5**	**3**	**50**	**1**	**0.1**	**22**	**62.5**	**45.052**	**211.8**	**180.9**	**231.298**
42.	**1**	**3**	**50**	**24**	**0.1**	**104.2**	**96.4**	**105.254**	**883.8**	**878.6**	**882.358**
43.	**1**	**9**	**20**	**24**	**100**	**871**	**813.2**	**877.877**	**173.4**	**237.9**	**201.272**
44.	**5**	**3**	**20**	**1**	**0.1**	**22.1**	**69.5**	**7.485**	**156.9**	**101.2**	**162.111**
45.	**5**	**9**	**20**	**1**	**100**	**125**	**90.8**	**92.611**	**32.4**	**30**	**−3.945**
46.	**5**	**3**	**50**	**24**	**0.1**	**7.5**	**−1.5**	**59.798**	**337.9**	**336.9**	**311.923**
47.	**1**	**9**	**20**	**1**	**100**	**454.2**	**490**	**484.253**	**70.7**	**61.1**	**31.574**
48.	**3**	**6**	**50**	**12.5**	**50**	**130.4**	**116.4**	**130.036**	**218.7**	**206.9**	**218.738**
49.	**1**	**3**	**50**	**24**	**100**	**623.1**	**646.5**	**624.234**	**149.5**	**137.8**	**144.84**
50.	**1**	**9**	**20**	**24**	**0.1**	**110.3**	**150.1**	**109.791**	**1143.3**	**1053.8**	**1140.1**

iterations. The best ANN architecture (5-8-8-2) contains 138 weights. The randomly distributed initial weights (±0.5) were transformed for the best model between −4.69 and 3.73. Based on these altered weights, we created a standalone user interface design shown in Fig. 5 to analyze the relationship between batch sorption process parameters and the removal of Ba(II)/Sr(II).

3. Results and discussion

3.1. Accuracy of best ANN model

Fig. 3 and Table 2 illustrated the comparison between the experimental and the predicted removal of Ba(II)/Sr(II) of the ANN model for the train, test, and total datasets. Adj. R^2 and Pearson's r are statistical approximations to illustrate how close the measured and predicted values. As illustrated in Fig. 3, in both the training and testing data sets, the ANN model shows superior prediction compared to the response surface methodology (RSM) model. The Pearson's and adj. R^2 values for the Ba(II) and Sr(II) removal by ANN model are 0.997, 0.994, 0.995, 0.991, and by the RSM model are 0.99, 0.981, 0.992, 0.983 respectively. We can conclude from these results that the present model was accurate than the RSM model (Younis et al., 2020) for the same data.

3.2. Comparison of the ANN model with the kinetic/isotherm models

Table 3 shows the comparison of correlation value (adj. R^2) between the kinetic, isotherm equations with the ANN model predictions. The seven nonlinear isotherm models based on two/three-parameter empirical equations have been applied to identify the batch sorption mechanisms. The models considered are RedlichePeterson (R–P), Langmuir (L), Freundlich (F), Toth (T), Temkin (TK), Langmuir-Freundlich (L-F), Dubinin-Radushjevich (D-R), and isotherms, as described in Table 3. Surface and intraparticle diffusion models (kinetic models) such as Intra-particle diffusion (IPD), Dumwald-Wagner (D.W.),

Table 3
Comparison of the ANN model with the various kinetic and isotherm models.

Sr. No	Kinetic/isotherm/ANN model	Equation	Adj. R-Squared		References
			Ba(II)	Sr(II)	
Isotherm models					
1	**R–P**	$q_e = \frac{K_R C_e}{[1+\alpha_R C_e^{n_R}}$	0.97	0.991	(Foo and Hameed, 2010; Younis et al., 2016)
2	**L**	$q_e = \frac{q_{m1} K_L C_e}{1+K_L C_e} (R_L = \frac{1}{1+K_L C_o})$	0.96	0.99	
3	**F**	$q_e = K_f C_e^{1/n}$	0.96	0.89	
4	**T**	$q_e = \frac{q_{m4} K_T C_e}{K_T C_e)(K_T C_e)(K_T C_e)^{1/n_T}]^{n_T}}$	0.975	0.992	
5	**T.K.**	$q_e = \frac{RT}{b_T} \ln K_{TK} C_e$	0.91	0.97	
6	**L-F**	$q_e = \frac{q_{m3} (K_{LF} C_e)^{1/m}}{1+(K_{LF} C_e)^{1/m}}$	0.98	0.99	
7	**D-R**	$q_e = q_{m2} \exp(-\mathrm{B}\ e^2)$ $e = RT \ln\left(1+\frac{1}{C_e}\right)\ E = \frac{1}{\sqrt{2B}}$	0.742	0.886	
Kinetic models					
8	**IPD**	$q_t = K_i t^{0.5} + C_i$	0.99	0.97	Younis et al. (2017)
9	**D.W.**	$Log(1-F^2) = -K_1/2.303t$	0.99	0.99	Klapiszewski et al. (2017)
10	**F.D.**	$Ln(1-F) = K_f t$	0.96	0.99	
11	**FPE**	$q_t = K_1 t^v$	0.91	0.856	Khambhaty et al. (2009)
12	**ANN model**		**0.994**	**0.991**	**Present work**

Film diffusion (F.D.), and fractional power equation (FPE) used for the prediction of removal efficiency. Compared with seven isotherm and four kinetic models, the ANN model predictions were more accurate in estimating the sorption process. Calculating the Ba(II)/Sr (II) sorption rate constants (varying with time) by kinetic and isotherm models require laborious calculations, whereas ANN model predictions are simple and effective. The developed user-friendly ANN model can predict the sorption efficiency without prior knowledge of neural networks with a single mouse click.

3.3. Single parameter sensitivity analysis on the removal of Ba(II)/Sr(II)

Fig. 4 shows the predicted effect of individual process parameters on removing Ba(II)/Sr(II) from TDS saline water by keeping other parameters at a constant value. Fig. 4(a) shows with an increase in biochar from 1 to 5.0 g/L resulted in a decrease in the Ba(II)/S(II) removal. The main reason for decreasing the sorption efficiency at high biochar amounts is due to an increase in the number of freely available active sites, and it will cause unsaturated Ba(II)/Sr(II) during the adsorption process (Gorzin and Bahri Rasht Abadi, 2018). From these results, we

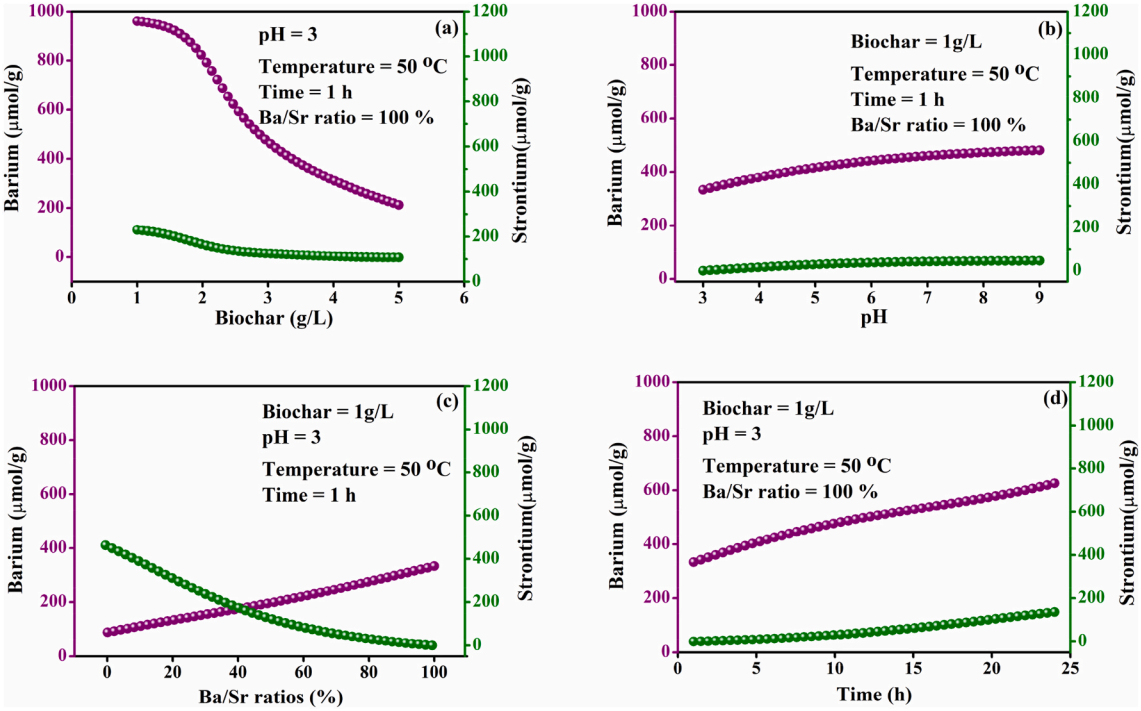

Fig. 4. Impact of individual process parameter on Ba(II)/Sr(II) sorption efficiency: (a) biochar, (b) pH, (c) Ba/Sr ratios, and (d) time.

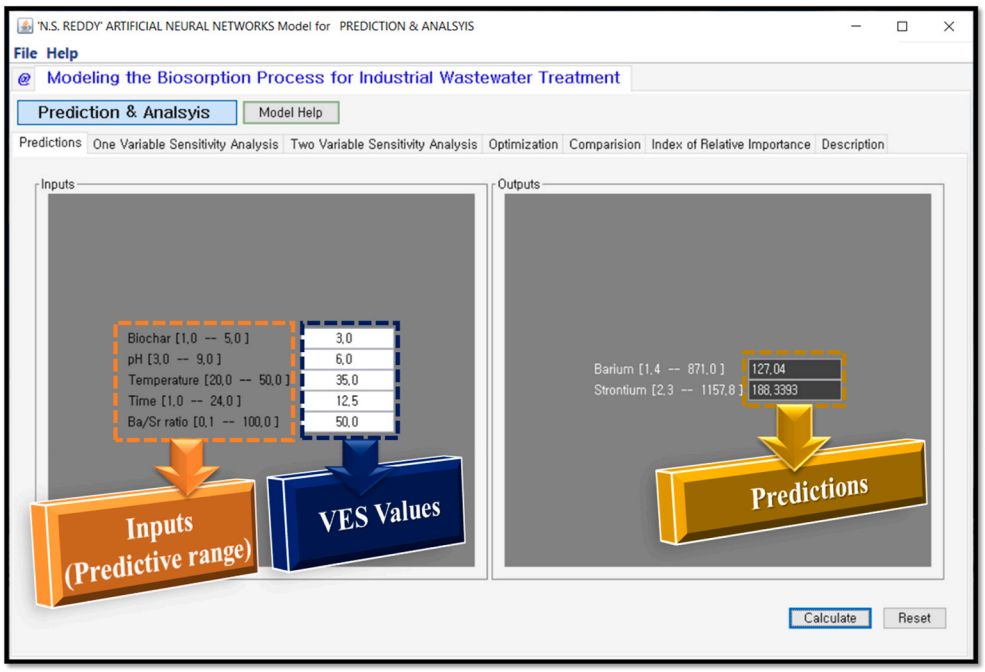

Fig. 5. The ANN model screenshot the prediction of barium and strontium removal for the mean process variables (virtual experimental system).

Table 4
Quantitative estimation of Ba(II)/Sr(II) sorption efficiency by Virtual Experimental System.

Biochar (g/L)	pH	Temp. (°C)	Time (h)	Ba/Sr ratio (%)	Sorption of Ba(II) (μmol/g)	Changed	Sorption of Sr(II) (μmol/g)	Changed
3	6	35	12.5	50	127.04	-	188.33	-
1	6	35	12.5	50	325.52	198.48	436.08	247.75
1	3	35	12.5	50	290.90	−34.62	221.20	−214.88
1	3	50	12.5	50	298.28	7.38	278.28	57.08
1	3	50	24	50	363.06	64.78	464.65	186.37
1	3	50	24	0.1	103.15	−259.91	879.15	414.5
Actual sorption of Ba and Sr values for the sample. 42.					104.2		883.8	

can conclude using small amounts of biochar will be sufficient in scale protection, i.e., in terms of its high affinity to uptake total Ba(II)/Sr(II). Fig. 4(b) displays the influence of pH on the sorption of Ba(II)/Sr(II); the sorption efficiency increased with the increase of pH from 3 to 9. At lower values of pH, the decrease in sorption efficiency is due to the positive charge density (H^+ or H_3O^+) on the biochar surface due to the high concentration of hydronium ions (H^+) in solution (Fard et al., 2017). This positively charged surface should have improved electrostatic repulsion, with Ba(II)/Sr(II) metal ions present in the forms of M^{2+} and $M(O.H.)^+$ at the edges of the biochar sorption sites (Fard et al., 2017). However, at high pH values (7–9), the negatively charged biochar surfaces were increased and increase the electrostatic attraction (i.e., O═C–O–Ba^{2+}-O-Si) of cationic Sr^{2+} and Ba^{2+} ions, thereby increasing the sorption of Ba(II)/Sr(II) from saline water (Ghaemi et al., 2011; Kaveeshwar et al., 2018; Mahfouz et al., 2015).

Fig. 4(c) illustrates the effect of varying Ba/Sr ratios from 0 to 100% on sorption efficiency. Increasing Ba/Sr ratios resulted in an increase in Ba(II) sorption efficiency and decreased Sr(II). It can be attributed to the surface activation and increases the Ba(II) sorption rate through the pore diffusion mechanism (Gorzin and Bahri Rasht Abadi, 2018). Fig. 4(d) explains the effect of time (1–24 h) on the sorption efficiency of Ba(II)/Sr(II) from the saline water. The sorption efficiency of Ba(II)/Sr(II) increases with increasing time (h). More than 12 h time is essential to raise the metal acceptance rate because it permits an incessant upsurge in the mass-transfer driving force necessary to achieve maximum equilibrium (monolayer occupation of sorption sites) (Fard et al., 2017).

3.4. Quantitative estimation by virtual experimental system (VES)

This section describes the study of the quantitative effect of process parameters on the sorption efficiency of Ba(II)/Sr(II) by altering virtually. We predicted the Ba(II)/Sr(II) 's removal for the database's mean values, and the values are similar to experimental observations. Table 4 illustrates the quantitative estimation of Ba(II)/Sr(II) sorption efficiency by the virtual addition of process parameters. The Ba(II) and Sr(II) sorption efficiency at the mean process parameters was predicted as 127.04 and 188.33, respectively. Fig. 5 illustrates the model's graphical user interface at the mean process variables. There are infinite combinations of possible experiments within the range of process parameters, and the model can predict with reasonable accuracy. To accomplish the experimental conditions of sample 42 (see Table 2), we changed the parameters virtually one by one. We estimated individual parameter effect quantitatively on the Ba(II)/Sr(II) removal using the model graphical user interface shown in Fig. 5.

As shown in Table 4, the decrease in the biochar from 3.0 to 1.0 g/L resulted in increasing sorption efficiency of Ba(II) and Sr(II) by 198.48 and 247.75 μmol/g, respectively. It means the decrease of every 1.0 g/L the sorption efficiency of Ba(II) and Sr(II) increases the 99.24 and 123.87 μmol/g, respectively. The pH reduction from 6 to 3 resulted in a marginal decrease in the Ba(II) and Sr(II) removal. The marginal decrease in removal is due to decreasing the electrostatic attraction of cationic Sr^{2+} and Ba^{2+} ions (Fard et al., 2017). An increase in the temperature from 35 to 50 °C increased in Ba(II) and Sr(II) removal by 7.38 and 57.08, respectively. The significant reduction of Sr(II) removal is

due to the higher mobility and lower density of the Sr(II) than the Ba(II) (Nishiyama et al., 2016). With an increase in the time from 12.5 to 24 h, the sorption efficiency was increased as expected. This could be attributed to the increasing monolayer occupation of sorption sites (Fard et al., 2017). Finally, with the increase in the Ba/Sr ratio from 50 to 0.1%, the Ba(II) removal was decreased rapidly; simultaneously, the Sr (II) removal was increased to 414.5 μmol/g. The virtual adding process parameters were reached to the experimental conditions of sample 42 (see Table 2). The calculated sorption efficiency of Ba(II)/Sr(II) is similar to the experimental Ba(II)/Sr(II) sorption efficiency of 104.2 and 883.8 μmol/g, respectively. This method identifies each process variable's influence quantitatively on Ba(II)/Sr(II) sorption efficiencies. The quantitative estimations agree with earlier predictions (Fig. 4). From these results, we can conclude that the developed ANN model can effectively predict the sorption efficiency of Ba(II)/Sr(II) from the wastewater.

4. Conclusions

The goal of this work is to model the relationships between the removal of Ba(II) and Sr(II) from the saline water as a function of five process parameters (biochar (g/L), pH, temperature (^{o}C), time (h), and Ba/Sr ratios) by ANN. The ANN models show superior results than kinetic and isotherm equations based on the correlation coefficients (adj. R^2 as 0.994 and 0.991 for Ba(II) and Sr(II) removal, respectively). Sensitivity analysis reveals the influence of process parameters on sorption efficiency. The developed graphical user interface is efficient in estimating the Ba(II)/Sr(II) sorption from the saline wastewater. The proposed virtual systems help reveal the relationship between process parameters and ions removal quantitatively.

Supplementary data

The supplementary files consist of ANN model development procedure, two-variable sensitivity analysis, qualitative estimation of the process parameters, and screenshots of the ANN model images' graphical user interfaces.

CRediT author statement

B.S.Reddy: Conceptualization and Writing- Original draft preparation, **A.K. Maurya:** Modeling, **V.E. Sathishkumar**: Writing and generation of the figures, **P. L Narayana:** Data collection and conceptualization, **M. H. Reddy:** Data Collection and English corrections, **Alaa Baazeem:** Reviewing and Editing, **Kwon-Koo Cho:** Writing Reviewing and Editing, and **N. S. Reddy:** Writing - Review & Editing, and supervision. All authors contributed to interpreting the results and provided critical feedback to the manuscript.

Declaration of competing interest

The authors declare that they have no known competing financial interests or personal relationships that could have appeared to influence the work reported in this paper.

Acknowledgments

N. S. Reddy acknowledges YSJ and ARNR for the Inspiration. All the Authors acknowledge YKK and J.K. for their help in the ANN model development. The authors extend their appreciation to Taif University for funding current work by Taif University Researchers Supporting Project number (TURSP-2020/295), Taif University, Taif, Saudi Arabia.

References

Al-Ghouti, M.A., et al., 2019. Produced water characteristics, treatment and reuse: a review. J. Water Process Eng. 28, 222–239.
Ayirala, S.C., et al., 2018. Microscopic scale interactions of water ions at crude oil/water interface and their impact on oil mobilization in advanced water flooding. J. Petrol. Sci. Eng. 163, 640–649.
Bukuaghangin, O., et al., 2016. Kinetics study of barium sulphate surface scaling and inhibition with a once-through flow system. J. Petrol. Sci. Eng. 147, 699–706.
El-Salamony, R., et al., 2017. Titania modified activated carbon prepared from sugarcane bagasse: adsorption and photocatalytic degradation of methylene blue under visible light irradiation. Environ. Technol. 38, 3122–3136.
Fakhru'l-Razi, A., et al., 2009. Review of technologies for oil and gas produced water treatment. J. Hazard Mater. 170, 530–551.
Fard, A.K., et al., 2017. Barium removal from synthetic natural and produced water using MXene as two dimensional (2-D) nanosheet adsorbent. Chem. Eng. J. 317, 331–342.
Foo, K.Y., Hameed, B.H., 2010. Insights into the modeling of adsorption isotherm systems. Chem. Eng. J. 156, 2–10.
Ghaemi, A., et al., 2011. Characterizations of strontium (II) and barium (II) adsorption from aqueous solutions using dolomite powder. J. Hazard Mater. 190, 916–921.
Gorzin, F., Bahri Rasht Abadi, M., 2018. Adsorption of Cr (VI) from aqueous solution by adsorbent prepared from paper mill sludge: kinetics and thermodynamics studies. Adsorpt. Sci. Technol. 36, 149–169.
Hasson, U., et al., 2020. Direct fit to nature: an evolutionary perspective on biological and artificial neural networks. Neuron 105, 416–434.
Hoseinian, F.S., et al., 2020. A hybrid neural network/genetic algorithm to predict Zn (II) removal by ion flotation. Separ. Sci. Technol. 55, 1197–1206.
Kamal, M.S., et al., 2018. Oilfield scale formation and chemical removal: a review. J. Petrol. Sci. Eng. 171, 127–139.
Katende, A., Sagala, F., 2019. A critical review of low salinity water flooding: mechanism, laboratory and field application. J. Mol. Liq. 278, 627–649.
Kaveeshwar, A.R., et al., 2018. Adsorption properties and mechanism of barium (II) and strontium (II) removal from fracking wastewater using pecan shell based activated carbon. J. Clean. Prod. 193, 1–13.
Khambhaty, Y., et al., 2009. Kinetics, equilibrium and thermodynamic studies on biosorption of hexavalent chromium by dead fungal biomass of marine Aspergillus Niger. Chem. Eng. J. 145, 489–495.
Klapiszewski, Ł., et al., 2017. Development of lignin based multifunctional hybrid materials for Cu (II) and Cd (II) removal from the aqueous system. Chem. Eng. J. 330, 518–530.
Li, L., et al., 2019. Biochar as a sorbent for emerging contaminants enables improvements in waste management and sustainable resource use. J. Clean. Prod. 210, 1324–1342.
Lippmann, R., 1987. An introduction to computing with neural nets. IEEE ASSP Mag. 4, 4–22.
Mahfouz, M.G., et al., 2015. Uranium extraction using magnetic nano-based particles of diethylenetriamine-functionalized chitosan: equilibrium and kinetic studies. Chem. Eng. J. 262, 198–209.
Mohubedu, R.P., et al., 2019. Magnetic valorization of biomass and biochar of a typical plant nuisance for toxic metals contaminated water treatment. J. Clean. Prod. 209, 1016–1024.
Nag, S., et al., 2020. Cr(VI) removal from aqueous solution using green adsorbents in continuous bed column – statistical and GA-ANN hybrid modelling. Chem. Eng. Sci. 226, 115904.
Nieva, A.D., et al., 2020. Prediction of adsorptive capacity of various agricultural wastes in the removal of heavy metals, dyes, and antibiotic in wastewater using ANN. Int. J. Environ. Sustain Dev. 11.
Nishiyama, Y., et al., 2016. Adsorption and removal of strontium in aqueous solution by synthetic hydroxyapatite. J. Radioanal. Nucl. Chem. 307, 1279–1285.
Prelot, B., et al., 2018. Contribution of calorimetry to the understanding of competitive adsorption of calcium, strontium, barium, and cadmium onto 4A type zeolite from two-metal aqueous solutions. Thermochim. Acta 664, 39–47.
Rashidi, N.A., Yusup, S., 2017. Potential of palm kernel shell as activated carbon precursors through single stage activation technique for carbon dioxide adsorption. J. Clean. Prod. 168, 474–486.
Reddy, B.R.S., et al., 2020. Modeling constituent–property relationship of polyvinylchloride composites by neural networks. Polym. Compos. 41, 3208–3217.
Reddy, B.S., et al., 2021a. Modeling tensile strength and suture retention of polycaprolactone electrospun nanofibrous scaffolds by artificial neural networks. Mater. Today Comm. 26, 102115.
Reddy, B.S., et al., 2021b. Modeling cyclic volatile methylsiloxanes removal efficiency from wastewater by ZnO-coated aluminum anode using artificial neural networks. J. King Saud Univ. Sci. 33, 101339.
Reddy, N., et al., 2015. Design of medium carbon steels by computational intelligence techniques. Comput. Mater. Sci. 101, 120–126.
Sadan, M.K., et al., 2016. Quantitative estimation of poly(methyl methacrylate) nanofiber membrane diameter by artificial neural networks. Eur. Polym. J. 74, 91–100.
Sivalingam, S., et al., 2019. Efficient sono-sorptive elimination of methylene blue by fly ash-derived nano-zeolite X: process optimization, isotherm and kinetic studies. J. Clean. Prod. 208, 1241–1254.
Yost, E.E., et al., 2016. Overview of chronic oral toxicity values for chemicals present in hydraulic fracturing fluids, flowback, and produced waters. Environ. Sci. Technol. 50, 4788–4797.
Younis, S.A., et al., 2016. Utilization of a pyrrole derivative based antimicrobial functionality impregnated onto CaO/gC 3 N 4 for dyes adsorption. RSC Adv. 6, 89367–89379.

Younis, S.A., et al., 2020. Use of rice straw-based biochar for batch sorption of barium/strontium from saline water: protection against scale formation in petroleum/desalination industries. J. Clean. Prod. 250, 119442.
Younis, S.A., et al., 2017. Modeling and optimization of oil adsorption from wastewater using an amorphous carbon thin film fabricated from wood sawdust waste modified with palmitic acid. Environ. Process. 4, 147–168.
Younis, S.A., Moustafa, Y.M., 2017. Synthesis of urea-modified MnFe 2 O 4 for aromatic micro-pollutants adsorption from wastewater: mechanism and modeling. Clean Technol. Environ. Policy 19, 527–540.
Zhai, S., et al., 2021. Cost-effective resource utilization for waste biomass: a simple preparation method of photo-thermal biochar cakes (B.C.s) toward dye wastewater treatment with solar energy. Environ. Res. 194, 110720.
Zhang, Z., et al., 2019. Effective treatment of shale oil and gas produced water by membrane distillation coupled with precipitative softening and walnut shell filtration. Desalination 454, 82–90.
Zhou, N., et al., 2019. Novel wet pyrolysis providing simultaneous conversion and activation to produce surface-functionalized biochars for cadmium remediation. J. Clean. Prod. 221, 63–72.